Dynamical Localization Transition of String Breaking in Quantum Spin Chains

Roberto Verdel,[1, 2, *] Guo-Yi Zhu,[1, 3, †] and Markus Heyl[1, 4, ‡]

[1] *Max Planck Institute for the Physics of Complex Systems, Nöthnitzer Straße 38, 01187 Dresden, Germany*
[2] *The Abdus Salam International Centre for Theoretical Physics, Strada Costiera 11, 34151 Trieste, Italy*
[3] *Institute for Theoretical Physics, University of Cologne, Zülpicher Straße 77, 50937 Cologne, Germany*
[4] *Center for Electronic Correlations and Magnetism,*
University of Augsburg, 86135 Augsburg, Germany
(Dated: December 11, 2023)

The fission of a string connecting two charges is an astounding phenomenon in confining gauge theories. The dynamics of this process have been studied intensively in recent years, with plenty of numerical results yielding a dichotomy: the confining string can decay relatively fast or persist up to extremely long times. Here, we put forward a dynamical localization transition as the mechanism underlying this dichotomy. To this end, we derive an effective string breaking description in the light-meson sector of a confined spin chain and show that the problem can be regarded as a dynamical localization transition in Fock space. Fast and suppressed string breaking dynamics are identified with delocalized and localized behavior, respectively. We then provide a further reduction of the dynamical string breaking problem onto a quantum impurity model, where the string is represented as an "impurity" immersed in a meson bath. It is shown that this model features a localization-delocalization transition, giving a general and simple physical basis to understand the qualitatively distinct string breaking regimes. These findings are directly relevant for a wider class of confining lattice models in any dimension and could be realized on present-day Rydberg quantum simulators.

Introduction.—The efficient implementation of gauge theories is a central target in quantum simulation [1–6], with some remarkable experimental realizations achieved in recent years [7–18]. However, the intrinsic structure of gauge theory still poses formidable technical challenges. Simultaneously, quantum spin chains, which are more amenable to quantum simulation, have been shown to be a versatile platform to emulate lattice gauge theory phenomenology. This has led to recent intensive efforts to investigate the structure of the gauge vacuum and out-of-equilibrium transport properties under the influence of confinement in this setting [19–40]. Yet, various aspects of such phenomena remain to be elucidated. In particular, numerical studies of dynamical string breaking—where a string connecting two charges decays due to pair production [41, 42]—suggest a dichotomy for the fate of the confining string: its fission can occur relatively fast or be substantially delayed.

In this Letter, we discuss how these observations can be interpreted in terms of an *underlying* dynamical localization transition. In this picture, the *localized phase* corresponds to a regime with a long-lived (prethermal) string, while the *delocalized phase* to fast string breaking. First, we show via exact diagonalization in quantum Ising chains that two qualitatively different string dynamics are separated by a sharp threshold in the long-time behavior of dynamical quantities. In particular, we study the survival probability and the half-chain entanglement entropy, with the former quantity serving as a direct diagnostics of string breaking. We then derive an effective model for the breaking of a short string by projecting onto a reduced subspace that captures resonant decay channels in the limit of vanishing transverse field. Within this effective description, string breaking can be

understood as a dynamical localization problem in Fock space. Next, this description is heuristically generalized to a quantum impurity model, where the string is effectively represented by a few-level system coupled to a meson bath. We show that this model features a dynamical localization-delocalization transition, with both sides of the transition explaining the observed string breaking regimes. This description, independent of microscopic details, provides a general and simple physical basis to understand dynamical string breaking. Finally, we discuss how our results can be applied to a wider class of confining lattice models in any dimension, and potential implementations with Rydberg quantum simulators.

String dynamics in quantum Ising chains.—We consider the quantum Ising model in both transverse (h_x) and longitudinal (h_z) fields, whose Hamiltonian for L spins on the ring reads

$$\hat{H} = -J \sum_{i=1}^{L} \hat{\sigma}_i^z \hat{\sigma}_{i+1}^z - h_x \sum_{i=1}^{L} \hat{\sigma}_i^x - h_z \sum_{i=1}^{L} \hat{\sigma}_i^z, \quad (1)$$

where $\hat{\sigma}_i^{x/z}$ are the Pauli matrices at site i, and $J > 0$ is the strength of a ferromagnetic coupling. The model (1) is of paramount importance in various fields—from statistical mechanics and condensed matter [43, 44] to high-energy physics [45–47]. Further, it can be naturally realized in present-day Rydberg quantum simulators [48–53], and solid-state materials [54]. Both integrability and $\mathbb{Z}_2$ symmetry are broken by a finite h_z, which induces a confining potential between pairs of domain wall (DW) excitations (provided that $h_x < J$). In this scenario, pairs of DWs form bound, mesonlike states. String breaking dynamics can then be probed by studying the stability of one such object under the unitary evolution generated
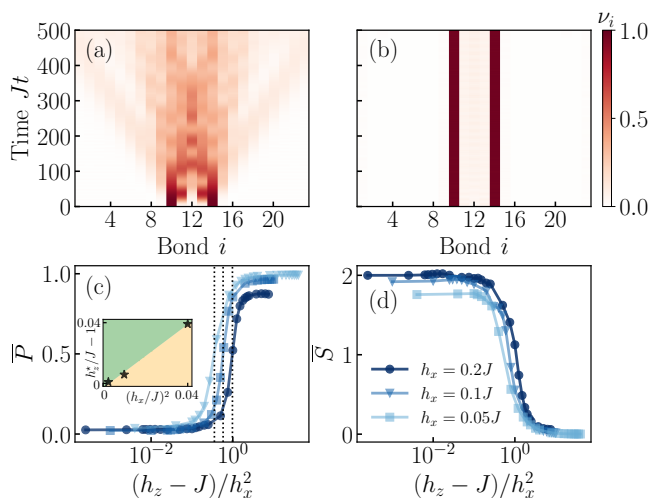
FIG. 1. String breaking dynamics in quantum Ising chains. (a) [$h_z = J$] Fast and (b) [$h_z = 1.1J$] suppressed string breaking dynamics in quantum Ising chains [Eq. (1)], in terms of the spatiotemporally resolved domain wall density $\nu_i(t)$. In both cases, $L = 24$, $h_x = 0.2J$ and $\ell = 4$ (initial string length). Long-time behavior of (c) the survival probability [Eq. (2)] and (d) half-chain entanglement entropy [Eq. (3)], for various values of the magnetic fields and $L = 16, \ell = 4$. A sharp threshold, defined by the point $h_z^\star/J$ where $\overline{P} = 0.5$ [dotted lines and inset in (c)], separates the two string breaking regimes. Results obtained via exact diagonalization.

by the Hamiltonian (1). Below, we review the main aspects of this process (see also Ref. [24]), in the confining regime with controlled quantum fluctuations $h_x \ll J$.

A dichotomy between distinct string breaking dynamics is revealed in a simple experimentally feasible quantum quench protocol. The system is initially prepared in a state with an Ising electric-field string of ℓ ↓-spins (in the σ^z basis) that connects two DWs, on top of the vacuum, i.e., $|\psi_{\text{string}}(\ell)\rangle \equiv |\cdots \uparrow\downarrow_{i_0}\downarrow\cdots\downarrow\downarrow_{(i_0+\ell-1)}\uparrow\cdots\rangle$. Next, the real-time evolution of the system in Eq. (1) is studied at finite h_x/J and h_z/J. Two qualitatively different dynamical string breaking scenarios are illustrated in Figs. 1(a) and 1(b), for an initial string of length $\ell = 4$. The dynamics are shown in terms of the local DW density, $\nu_i(t) = \frac{1}{2}\langle \hat{I} - \hat{\sigma}_i^z(t)\hat{\sigma}_{i+1}^z(t)\rangle$, defined on the bonds between consecutive lattice sites. In Fig. 1(a), a rapid production of new DW pairs occurs inside the string, eventually leading to its decay and emission of lighter mesons. A subsequent proliferation of DW pairs throughout the whole chain eventually restores translation invariance, in agreement with the fact that the system (1) is ergodic and thermalizing at late times [55]. This *fast* string breaking dynamics can be understood as a consequence of underlying resonances that arise for commensurable (J, h_z) [24, 56]. In sharp contrast, the rapid string breaking dynamics is surprisingly absent in Fig. 1(b), up to the accessed long time $O(10^2 J^{-1})$, which is also beyond the

timescale for light meson kinetics $t \gg J/h_x^2$. Based on general thermalization arguments (as mentioned above), the latter regime must be understood only as a prethermal phenomenon [34].

The scenarios above have been observed in both quantum spin models [21, 24, 25] and low-dimensional lattice gauge theories [57–62]. However, a general picture of how these systems cross from one regime over to the other remains to be provided. As a first step in this quest, we study the long-time behavior of the string survival probability

$$P(t) = |\langle\psi_{\text{string}}|\psi(t)\rangle|^2, \qquad (2)$$

and the half-chain entanglement entropy

$$S(t) = S(\hat{\rho}_A(t)) = -\text{Tr}_A[\hat{\rho}_A(t)\ln\hat{\rho}_A(t)], \qquad (3)$$

where $|\psi(t)\rangle$ is the time-evolved many-body wave function and $\hat{\rho}_A(t) = \text{Tr}_B[|\psi(t)\rangle\langle\psi(t)|]$ is the reduced density matrix computed on one half of the chain (cutting through the middle of the string and the opposite point on the periodic chain). We compute long-time averages as $\overline{\mathcal{O}} = \frac{1}{t_f - t_i}\int_{t_i}^{t_f}\mathcal{O}(t)\text{d}t$. In our calculations we take $Jt_f = 10^4$, and $Jt_i = 3Jt_{\text{sb}}$, where $Jt_{\text{sb}} \equiv \frac{\pi}{2(h_x/J)^2}$ is a typical timescale for string breaking [24]. The long-time averages of the quantities in Eqs. (2) and (3) are shown in Figs. 1(c) and 1(d), for various values of h_z/J and h_x/J. We observe a sharp threshold—defined by the point where $\overline{P} = 0.5$—, which roughly scales linearly with $(h_x/J)^2$ [inset in Fig. 1(c)], and separates a regime where the string breaks ($\overline{P} \sim 0$) from one in which it persists up to the accessed timescales ($\overline{P} \sim 1$). The behavior of $\overline{S}$ shows that string breaking is characterized by a significant amount of entanglement, while in *suppressed* string breaking dynamics entanglement production is strongly diminished.

String breaking as a localization problem in Fock space.—We now derive an effective description of the above phenomenology. Let us fix $\ell = 4$, as before. For the considered parameter regime $h_x \ll h_z \sim J$, one can systematically project out sectors of the Hilbert space that do not participate in resonant decay channels, by applying a Schrieffer-Wolff transformation [63, 64] to (1), see Ref. [65] for details. Here, the relevant physical subspace is formed by the direct sum of the "string" sector and the "1-meson pair" sector, see Fig. 2(a). The former sector is spanned by the kets $|S_j\rangle = |\cdots \uparrow\uparrow\downarrow_j\downarrow\downarrow\uparrow\uparrow \cdots\rangle$, with a string of size $\ell = 4$, labelled by the site index j of the first ↓-spin. The second sector comprises configurations with exactly two 1-meson particles: $|j, d\rangle = |\cdots \uparrow\uparrow\downarrow_j\uparrow \cdots \uparrow\downarrow_{(j+d)}\uparrow\uparrow \cdots\rangle$, where $2 \leq d \leq L/2$ (L even), is the relative distance between the two ↓-spins.

The resulting effective model reads:

$$\hat{H}_{\text{eff}} = \hat{H}_{\text{string}} + \hat{H}_{\text{mesons}} + \hat{H}_\lambda, \qquad (4)$$
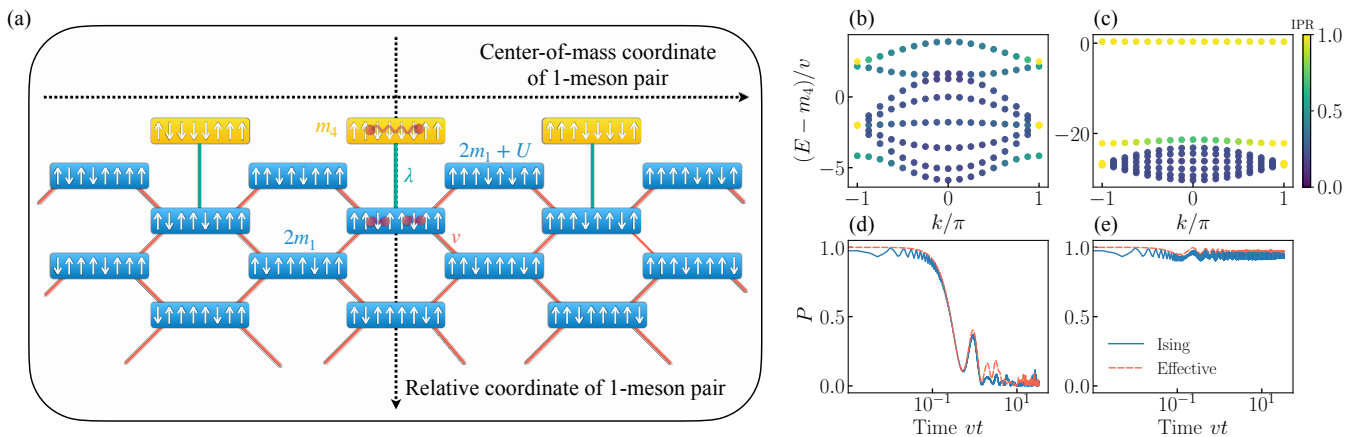
FIG. 2. Effective graph model for string breaking dynamics. (a) Schematic of the effective model for a short string ($\ell = 4$). Spin configurations in yellow represent string states (rest mass $m_4 = 12J$), whereas configurations in blue represent 1-meson pairs with energy $2m_1$ and hopping amplitude $v = h_x^2/3J$ (red bonds). These are the configurations involved, to leading order, in the resonant decay of the string (green bonds). For illustration, confined DW pairs are depicted in some configurations as red dots joined by a wiggly line. String breaking can thus be thought of as a diffusion problem in the Fock-space graph. (b),(c) Energy spectrum of the effective model for $h_z = J$ and $h_z = 1.02J$, respectively. In (b) all bands have a similar energy, while in (c) there is a gap between the "string" band and the continuum of 1-meson pairs. Colorbar shows the IPR of individual eigenstates [Eq. (5)], exhibiting a strong localization of the string modes in the latter case. (d),(e) Time evolution of the survival probability [Eq. (2)], for the respective parameters, both in the effective and full Ising model. Note the log scale in the horizontal axis and the time in unit of v. Parameters: $L = 16, h_x = 0.1J$.

where $\hat{H}_{\text{string}}$ gives the string rest mass [$\mathcal{E}_s \equiv m_4 = 12J$]; $\hat{H}_{\text{mesons}}$ contains terms for hopping [$v = h_x^2/(3J)$], mass [$2m_1 = \mathcal{E}_s - 2v$], and repulsive contact interaction [$U = 9v/2$] of the 1-meson particles; and $\hat{H}_\lambda$ couples the two relevant sectors with amplitude $\lambda = -3v$; see Fig. 2(a) and Ref. [65] for details. The latter term is responsible for the processes of pair creation and recombination, and therefore, crucial for string breaking.

The energy spectrum of this model is shown in Figs. 2(b) and 2(c), for different choices of parameters. In Fig. 2(b) all bands are close in energy, while in Fig. 2(c) a large gap separates an isolated band (associated to string modes) from the rest. In the latter case, string modes are strongly localized. This is quantified by the colorbar in Figs. 2(b) and 2(c), which shows the value of the inverse participation ratio (IPR) of individual energy eigenstates:

$$\text{IPR}(n) = \sum_a |\langle a|n\rangle|^4, \qquad (5)$$

where $\{|n\rangle\}$ are eigenstates of $\hat{H}_{\text{eff}}$ and $\{|a\rangle\}$ preferential basis states. Localized behavior of $|n\rangle$ occurs when $\text{IPR}(n) \simeq 1$, while $\text{IPR}(n)$ vanishes as $1/D$ in the maximally delocalized case, where D is the Hilbert space dimension [66].

The evolution of the survival probability [Eq. (2)], corresponding to the two cases above, is shown in Figs. 2(d) and 2(e). While in the former case, the string eventually breaks ($P \sim 0$), in the latter it survives ($P \sim 1$) up to long times. The spectra in Figs. 2(b) and 2(c) are hence

identified with fast and suppressed string breaking dynamics, respectively. String breaking can thus be seen as a dynamical localization problem in the Fock-space graph in Fig. 2(a), where the string localizes if it is not resonantly coupled to the continuum of 1-meson pairs. Quantitative agreement with the dynamics in the full Ising model is also observed in Figs. 2(d) and 2(e), which can be systematically improved by decreasing h_x/J [65].

Quantum impurity model picture.—The above picture resembles localization phenomena in quantum impurity models (QIMs) [67–69]. This is the basis for a further reduction of the string breaking problem. Let us consider an elementary string breaking/fusion process: $(\cdots \uparrow\uparrow\downarrow\downarrow\downarrow\downarrow\downarrow\uparrow\uparrow \cdots)_i \longleftrightarrow (\cdots \uparrow\uparrow\downarrow\downarrow\downarrow\uparrow\downarrow\uparrow\uparrow \cdots)_{ii} \longleftrightarrow (\cdots \uparrow\uparrow\downarrow\downarrow\uparrow\uparrow \cdots \uparrow\downarrow\uparrow \cdots)_{iii}$, where a string ($i$) gets cut near its edges via pair creation, yielding a *metastable* configuration (ii), and eventually, a shorter string plus a 1-meson (iii) [58, 62]. We encode the different configurations of this basic process in the internal states of a spin-1 system ("impurity"). Concretely, we map the symmetric and antisymmetric string states $\frac{1}{\sqrt{2}} [|\psi_{\text{string}}\rangle \pm |\psi_{\text{meta}}\rangle]$, onto the impurity states $|S^z = \pm 1\rangle$, respectively, and the state where the string has been cut and a lighter meson radiated onto $|S^z = 0\rangle$. The impurity is also locally coupled to a meson bath in analogy to the picture in Fig. 2(a). This motivates a QIM with Hamiltonian

$$\hat{H}_{\text{QIM}} = \hat{H}_{\text{imp}} + \hat{H}_{\text{bath}} + \hat{H}_{\text{coup}}, \qquad (6)$$

where $\hat{H}_{\text{imp}} = (M - \mu)(\hat{S}^z)^2 + \Lambda \hat{S}^z$, contains the string mass term M, a chemical potential μ accounting for
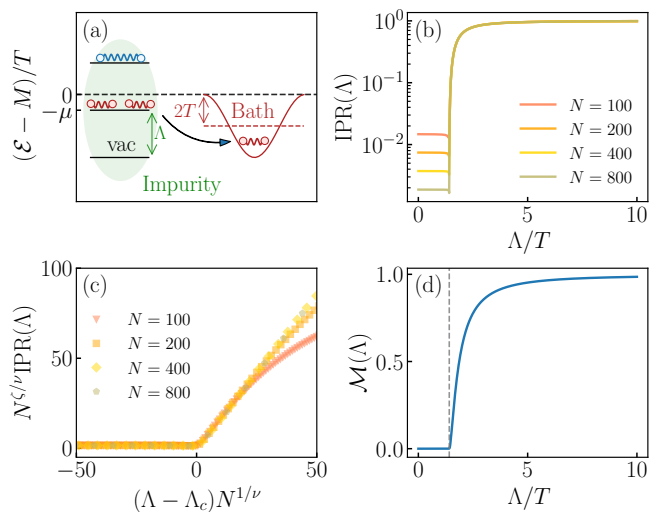
FIG. 3. Localization-delocalization transition in the QIM. (a) Minimal string breaking/fusion as a three-level system (impurity), coupled to a bath. The impurity-bath coupling may or may not be resonant, yielding hybridization (as depicted here)—corresponding to string decay—or localization, respectively. (b) IPR of the impurity mode as a function of Λ/T, for various system sizes, displaying a localization-delocalization transition. (c) Data collapse of the data in (b) using a standard finite-size scaling ansatz within the package `pyfssa` [71], yielding $\Lambda_c/T = 1.41(1)$ and critical exponents $\zeta = 1.02(5)$, $\nu = 1.00(5)$. (d) Long-time average of the spin autocorrelation function $\mathcal{M}(\Lambda)$, as a function of Λ/T with $N = 800$. The dashed line indicates the transition point $\Lambda_c/T \approx 1.41$. Parameters: $M/T = 10$, $\mu/T = 2$.

higher-order corrections, and a $\Lambda > 0$ term, directly related to string breaking/fusion; $\hat{H}_{\text{bath}} = \sum_{j=1}^{N} \big[- T(\hat{b}_j^\dagger \hat{b}_{j+1} + \text{h.c.}) + (M - 2T)\hat{b}_j^\dagger \hat{b}_j \big]$, describes a bath of light mesons represented by hard-core bosons with creation (annihilation) operators $\hat{b}_j^\dagger$ ($\hat{b}_j$), on a chain with N sites, with hopping amplitude $-T$ and maximal kinetic energy $M - 2T$; and $\hat{H}_{\text{coup}} = -T\big[\big(1 - (\hat{S}^z)^2\big)\hat{S}^x\hat{b}_1^\dagger + \text{h.c.}\big]$, couples the impurity with the bath such that if $|S^z = 0\rangle$ a meson at site 1 is created, and whenever $|S^z = \pm 1\rangle$ a meson at that site is annihilated [70].

A schematic of this mapping is shown in Fig. 3(a) for a short string that can decay into two shorter strings. The latter can be emitted into a meson bath, if the impurity-bath coupling is resonant, leaving the impurity in its "vacuum" state. Otherwise, the shorter strings can recombine back into a longer string, avoiding its decay. This QIM picture thus offers a distilled abstraction of the effective graph model in Fig. 2(a). We note, however, that the mapping between these two models is not exact. Yet, as shown below, both models have significant similarities both in the behavior of their eigenstates as well as in the dynamics of the impurity and the string.

The QIM in Eq. (6) features a localization-delocalization transition, explicitly shown in the single-

meson limit. In this limit the spin can be replaced by two hard-core bosons, and due to particle number conservation, exact diagonalization is possible for large system sizes [65]. Focusing on the IPR of individual eigenstates, we see that the impurity mode can abruptly localize when varying Λ/T above a critical Λ_c/T, see Fig. 3(b), while the IPR of bulk eigenstates always vanishes (not shown). A standard finite-size scaling analysis [72], see Fig. 3(c), yields $\Lambda_c/T = 1.41(1)$ and critical exponents $\zeta = -1.02(5)$, $\nu = 1.00(5)$, for the considered parameters.

Such localization-delocalization transition underlies and governs two qualitatively different spin dynamics, see Fig. 3(d). Here we plot the long-time averaged spin autocorrelation function $\mathcal{M}(\Lambda) = \lim_{t\to\infty} \frac{1}{t}\int_0^t dt' \langle \hat{S}^z(t')\hat{S}^z(0)\rangle_\Lambda$, where $\langle \cdot \rangle_\Lambda$ denotes the expectation value at a given Λ/T. This quantity plays an equivalent role to the survival probability for the spin chain [Eq. (2)], and likewise, it vanishes on the delocalized side of the transition, while it approaches unity as we ramp up Λ/T, above the localization transition point.

Our conclusions are restricted to the lattice as we have only considered a bounded spectrum of excitations. We expect our observations to hold beyond the limit $h_x \ll J$, as long as there exist values of h_z/J for which certain decay channels lead to faster dynamics than in other regimes. We note that our effective descriptions are valid only within the prethermal timescale of the localized regime. Also, further localization transitions may occur around other resonance points of the spin chain, which could involve longer decay paths [24, 32], and hence, would require to consider an impurity with more internal levels. Regarding the Fock-space graph model, we note that adding higher-order corrections could reshape the transition path and change the criticality. Nevertheless, as the effect of such higher-order terms is just a renormalization of hopping amplitudes [25], we expect the physics to remain qualitatively unaltered far from the localization transition point and deep in the two phases.

Discussion and outlook.—We expect our main results to be relevant for a wider class of confining theories in one and higher dimensions. In effect, what seems to be crucial in the applicability of the QIM picture is that the system retains rotational symmetry, with the radial coordinate effectively defining a one-dimensional problem, when integrating out the rotation degree of freedom [68]. Fermionic bound states (e.g., baryons) could also be accounted for by changing the statistics of the bath [68, 69]. Finally, our observations can be experimentally realized with current quantum technologies. In particular, Rydberg atoms offer a well suited platform, in which both the initial string states and the target unitary dynamics can be implemented in a highly controllable way [48–53].

----

* rverdel@ictp.it
† gzhu@uni-koeln.de
‡ markus.heyl@uni-a.de

[1] U.-J. Wiese, "Ultracold quantum gases and lattice systems: quantum simulation of lattice gauge theories," Annalen der Physik **525**, 777–796 (2013), https://onlinelibrary.wiley.com/doi/pdf/10.1002/andp.201300104.

[2] Erez Zohar, J Ignacio Cirac, and Benni Reznik, "Quantum simulations of lattice gauge theories using ultracold atoms in optical lattices," Reports on Progress in Physics **79**, 014401 (2015).

[3] Mari Carmen Bañuls, Rainer Blatt, Jacopo Catani, Alessio Celi, Juan Ignacio Cirac, Marcello Dalmonte, Leonardo Fallani, Karl Jansen, Maciej Lewenstein, Simone Montangero, Christine A. Muschik, Benni Reznik, Enrique Rico, Luca Tagliacozzo, Karel Van Acoleyen, Frank Verstraete, Uwe-Jens Wiese, Matthew Wingate, Jakub Zakrzewski, and Peter Zoller, "Simulating lattice gauge theories within quantum technologies," The European Physical Journal D **74**, 165 (2020).

[4] Natalie Klco, Alessandro Roggero, and Martin J Savage, "Standard model physics and the digital quantum revolution: Thoughts about the interface," Reports on Progress in Physics (2022).

[5] Monika Aidelsburger, Luca Barbiero, Alejandro Bermudez, Titas Chanda, Alexandre Dauphin, Daniel González-Cuadra, Przemysław R. Grzybowski, Simon Hands, Fred Jendrzejewski, Johannes Jünemann, Gediminas Juzeliūnas, Valentin Kasper, Angelo Piga, Shi-Ju Ran, Matteo Rizzi, Germán Sierra, Luca Tagliacozzo, Emanuele Tirrito, Torsten V. Zache, Jakub Zakrzewski, Erez Zohar, and Maciej Lewenstein, "Cold atoms meet lattice gauge theory," Philosophical Transactions of the Royal Society A: Mathematical, Physical and Engineering Sciences **380**, 20210064 (2022), https://royalsocietypublishing.org/doi/pdf/10.1098/rsta.2021.0064.

[6] L. Funcke, T. Hartung, K. Jansen, S. Kühn, M. Schneider, P. Stornati, and X. Wang, "Towards quantum simulations in particle physics and beyond on noisy intermediate-scale quantum devices," Philosophical Transactions of the Royal Society A: Mathematical, Physical and Engineering Sciences **380**, 20210062 (2022), https://royalsocietypublishing.org/doi/pdf/10.1098/rsta.2021.0062.

[7] Esteban A. Martinez, Christine A. Muschik, Philipp Schindler, Daniel Nigg, Alexander Erhard, Markus Heyl, Philipp Hauke, Marcello Dalmonte, Thomas Monz, Peter Zoller, and Rainer Blatt, "Real-time dynamics of lattice gauge theories with a few-qubit quantum computer," Nature **534**, 516–519 (2016).

[8] Han-Ning Dai, Bing Yang, Andreas Reingruber, Hui Sun, Xiao-Fan Xu, Yu-Ao Chen, Zhen-Sheng Yuan, and Jian-Wei Pan, "Four-body ring-exchange interactions and anyonic statistics within a minimal toric-code hamiltonian," Nature Physics **13**, 1195–1200 (2017).

[9] Logan W. Clark, Brandon M. Anderson, Lei Feng, Anita Gaj, K. Levin, and Cheng Chin, "Observation of density-dependent gauge fields in a bose-einstein condensate based on micromotion control in a shaken two-dimensional lattice," Phys. Rev. Lett. **121**, 030402 (2018).

[10] N. Klco, E. F. Dumitrescu, A. J. McCaskey, T. D. Morris, R. C. Pooser, M. Sanz, E. Solano, P. Lougovski, and M. J. Savage, "Quantum-classical computation of schwinger model dynamics using quantum computers," Phys. Rev. A **98**, 032331 (2018).

[11] C. Kokail, C. Maier, R. van Bijnen, T. Brydges, M. K. Joshi, P. Jurcevic, C. A. Muschik, P. Silvi, R. Blatt, C. F. Roos, and P. Zoller, "Self-verifying variational quantum simulation of lattice models," Nature **569**, 355–360 (2019).

[12] Frederik Görg, Kilian Sandholzer, Joaquín Minguzzi, Rémi Desbuquois, Michael Messer, and Tilman Esslinger, "Realization of density-dependent peierls phases to engineer quantized gauge fields coupled to ultracold matter," Nature Physics **15**, 1161–1167 (2019).

[13] Christian Schweizer, Fabian Grusdt, Moritz Berngruber, Luca Barbiero, Eugene Demler, Nathan Goldman, Immanuel Bloch, and Monika Aidelsburger, "Floquet approach to z_2 lattice gauge theories with ultracold atoms in optical lattices," Nature Physics **15**, 1168–1173 (2019).

[14] Alexander Mil, Torsten V. Zache, Apoorva Hegde, Andy Xia, Rohit P. Bhatt, Markus K. Oberthaler, Philipp Hauke, Jürgen Berges, and Fred Jendrzejewski, "A scalable realization of local u(1) gauge invariance in cold atomic mixtures," Science **367**, 1128–1130 (2020), https://www.science.org/doi/pdf/10.1126/science.aaz5312.

[15] Bing Yang, Hui Sun, Robert Ott, Han-Yi Wang, Torsten V. Zache, Jad C. Halimeh, Zhen-Sheng Yuan, Philipp Hauke, and Jian-Wei Pan, "Observation of gauge invariance in a 71-site bose–hubbard quantum simulator," Nature **587**, 392–396 (2020).

[16] Zhao-Yu Zhou, Guo-Xian Su, Jad C. Halimeh, Robert Ott, Hui Sun, Philipp Hauke, Bing Yang, Zhen-Sheng Yuan, Jürgen Berges, and Jian-Wei Pan, "Thermalization dynamics of a gauge theory on a quantum simulator," Science **377**, 311–314 (2022), https://www.science.org/doi/pdf/10.1126/science.abl6277.

[17] G. Semeghini, H. Levine, A. Keesling, S. Ebadi, T. T. Wang, D. Bluvstein, R. Verresen, H. Pichler, M. Kalinowski, R. Samajdar, A. Omran, S. Sachdev, A. Vishwanath, M. Greiner, V. Vuletić, and M. D. Lukin, "Probing topological spin liquids on a programmable quantum simulator," Science **374**, 1242–1247 (2021), https://www.science.org/doi/pdf/10.1126/science.abi8794.

[18] K. J. Satzinger, Y.-J Liu, A. Smith, C. Knapp, M. Newman, C. Jones, Z. Chen, C. Quintana, X. Mi, A. Dunsworth, C. Gidney, I. Aleiner, F. Arute, K. Arya, J. Atalaya, R. Babbush, J. C. Bardin, R. Barends, J. Basso, A. Bengtsson, A. Bilmes, M. Broughton, B. B. Buckley, D. A. Buell, B. Burkett, N. Bushnell, B. Chiaro, R. Collins, W. Courtney, S. Demura, A. R. Derk, D. Eppens, C. Erickson, L. Faoro, E. Farhi, A. G. Fowler, B. Foxen, M. Giustina, A. Greene, J. A. Gross, M. P. Harrigan, S. D. Harrington, J. Hilton, S. Hong, T. Huang, W. J. Huggins, L. B. Ioffe, S. V. Isakov, E. Jeffrey, Z. Jiang, D. Kafri, K. Kechedzhi, T. Khattar, S. Kim, P. V. Klimov, A. N. Korotkov, F. Kostritsa, D. Landhuis, P. Laptev, A. Locharla, E. Lucero,

O. Martin, J. R. McClean, M. McEwen, K. C. Miao, M. Mohseni, S. Montazeri, W. Mruczkiewicz, J. Mutus, O. Naaman, M. Neeley, C. Neill, M. Y. Niu, T. E. O'Brien, A. Opremcak, B. Pató, A. Petukhov, N. C. Rubin, D. Sank, V. Shvarts, D. Strain, M. Szalay, B. Villalonga, T. C. White, Z. Yao, P. Yeh, J. Yoo, A. Zalcman, H. Neven, S. Boixo, A. Megrant, Y. Chen, J. Kelly, V. Smelyanskiy, A. Kitaev, M. Knap, F. Pollmann, and P. Roushan, "Realizing topologically ordered states on a quantum processor," Science **374**, 1237–1241 (2021), https://www.science.org/doi/pdf/10.1126/science.abi8378.

[19] M. Kormos, M. Collura, G. Takács, and P. Calabrese, "Real-time confinement following a quantum quench to a non-integrable model," Nat. Phys. **13**, 246 (2017).

[20] Fangli Liu, Rex Lundgren, Paraj Titum, Guido Pagano, Jiehang Zhang, Christopher Monroe, and Alexey V. Gorshkov, "Confined quasiparticle dynamics in long-range interacting quantum spin chains," Phys. Rev. Lett. **122**, 150601 (2019).

[21] Paolo Pietro Mazza, Gabriele Perfetto, Alessio Lerose, Mario Collura, and Andrea Gambassi, "Suppression of transport in nondisordered quantum spin chains due to confined excitations," Phys. Rev. B **99**, 180302(R) (2019).

[22] Alessio Lerose, Bojan Žunkovič, Alessandro Silva, and Andrea Gambassi, "Quasilocalized excitations induced by long-range interactions in translationally invariant quantum spin chains," Phys. Rev. B **99**, 121112(R) (2019).

[23] Andrew J. A. James, Robert M. Konik, and Neil J. Robinson, "Nonthermal states arising from confinement in one and two dimensions," Phys. Rev. Lett. **122**, 130603 (2019).

[24] Roberto Verdel, Fangli Liu, Seth Whitsitt, Alexey V. Gorshkov, and Markus Heyl, "Real-time dynamics of string breaking in quantum spin chains," Phys. Rev. B **102**, 014308 (2020).

[25] Alessio Lerose, Federica M. Surace, Paolo P. Mazza, Gabriele Perfetto, Mario Collura, and Andrea Gambassi, "Quasilocalized dynamics from confinement of quantum excitations," Phys. Rev. B **102**, 041118(R) (2020).

[26] Riccardo Javier Valencia Tortora, Pasquale Calabrese, and Mario Collura, "Relaxation of the order-parameter statistics and dynamical confinement," Europhysics Letters **132**, 50001 (2020).

[27] Aritra Sinha, Titas Chanda, and Jacek Dziarmaga, "Nonadiabatic dynamics across a first-order quantum phase transition: Quantized bubble nucleation," Phys. Rev. B **103**, L220302 (2021).

[28] Federica Maria Surace and Alessio Lerose, "Scattering of mesons in quantum simulators," New Journal of Physics **23**, 062001 (2021).

[29] Gianluca Lagnese, Federica Maria Surace, Márton Kormos, and Pasquale Calabrese, "False vacuum decay in quantum spin chains," Phys. Rev. B **104**, L201106 (2021).

[30] Gianluca Lagnese, Federica Maria Surace, Márton Kormos, and Pasquale Calabrese, "Quenches and confinement in a heisenberg–ising spin ladder," Journal of Physics A: Mathematical and Theoretical **55**, 124003 (2022).

[31] Stefano Scopa, Pasquale Calabrese, and Alvise Bastianello, "Entanglement dynamics in confining spin chains," Phys. Rev. B **105**, 125413 (2022).

[32] P. I. Karpov, G.-Y. Zhu, M. P. Heller, and M. Heyl, "Spatiotemporal dynamics of particle collisions in quantum spin chains," Phys. Rev. Research **4**, L032001 (2022).

[33] Ashley Milsted, Junyu Liu, John Preskill, and Guifre Vidal, "Collisions of false-vacuum bubble walls in a quantum spin chain," PRX Quantum **3**, 020316 (2022).

[34] Stefan Birnkammer, Alvise Bastianello, and Michael Knap, "Prethermalization in one-dimensional quantum many-body systems with confinement," Nature Communications **13**, 7663 (2022).

[35] Mario Collura, Andrea De Luca, Davide Rossini, and Alessio Lerose, "Discrete time-crystalline response stabilized by domain-wall confinement," Phys. Rev. X **12**, 031037 (2022).

[36] Joseph Vovrosh, Rick Mukherjee, Alvise Bastianello, and Johannes Knolle, "Dynamical hadron formation in long-range interacting quantum spin chains," PRX Quantum **3**, 040309 (2022).

[37] Alvise Bastianello, Umberto Borla, and Sergej Moroz, "Fragmentation and emergent integrable transport in the weakly tilted ising chain," Phys. Rev. Lett. **128**, 196601 (2022).

[38] W. L. Tan, P. Becker, F. Liu, G. Pagano, K. S. Collins, A. De, L. Feng, H. B. Kaplan, A. Kyprianidis, R. Lundgren, W. Morong, S. Whitsitt, A. V. Gorshkov, and C. Monroe, "Domain-wall confinement and dynamics in a quantum simulator," Nature Physics **17**, 742–747 (2021).

[39] Joseph Vovrosh and Johannes Knolle, "Confinement and entanglement dynamics on a digital quantum computer," Scientific Reports **11**, 11577 (2021).

[40] Christopher Lamb, Yicheng Tang, Robert Davis, and Ananda Roy, "Ising Meson Spectroscopy on a Noisy Digital Quantum Simulator," arXiv e-prints , arXiv:2303.03311 (2023), arXiv:2303.03311 [quant-ph].

[41] Gunnar S. Bali, Hartmut Neff, Thomas Düssel, Thomas Lippert, and Klaus Schilling (SESAM Collaboration), "Observation of string breaking in qcd," Phys. Rev. D **71**, 114513 (2005).

[42] F. Hebenstreit, J. Berges, and D. Gelfand, "Real-time dynamics of string breaking," Phys. Rev. Lett. **111**, 201601 (2013).

[43] Barry M. McCoy and Tai Tsun Wu, *The Two-Dimensional Ising Model* (Harvard University Press, 1973).

[44] Subir Sachdev, *Quantum Phase Transitions*, 2nd ed. (Cambridge University Press, Cambridge, 2011).

[45] Barry M. McCoy and Tai Tsun Wu, "Two-dimensional ising field theory in a magnetic field: Breakup of the cut in the two-point function," Phys. Rev. D **18**, 1259–1267 (1978).

[46] Barry M. McCoy and Tai Tsun Wu, "Speculations on quark observation," Physics Letters B **72**, 219–223 (1977).

[47] Barry M. McCoy and Jean-Marie Maillard, "The Importance of the Ising Model," Progress of Theoretical Physics **127**, 791–817 (2012).

[48] Hannes Bernien, Sylvain Schwartz, Alexander Keesling, Harry Levine, Ahmed Omran, Hannes Pichler, Soonwon Choi, Alexander S. Zibrov, Manuel Endres, Markus Greiner, Vladan Vuletić, and Mikhail D. Lukin, "Probing many-body dynamics on a 51-atom quantum simulator," Nature **551**, 579–584 (2017).

[49] Matteo Marcuzzi, Ji ří Minář, Daniel Barredo, Sylvain

de Léséleuc, Henning Labuhn, Thierry Lahaye, Antoine Browaeys, Emanuele Levi, and Igor Lesanovsky, "Facilitation dynamics and localization phenomena in rydberg lattice gases with position disorder," Phys. Rev. Lett. **118**, 063606 (2017).

[50] Johannes Zeiher, Jae-yoon Choi, Antonio Rubio-Abadal, Thomas Pohl, Rick van Bijnen, Immanuel Bloch, and Christian Gross, "Coherent many-body spin dynamics in a long-range interacting ising chain," Phys. Rev. X **7**, 041063 (2017).

[51] Vincent Lienhard, Sylvain de Léséleuc, Daniel Barredo, Thierry Lahaye, Antoine Browaeys, Michael Schuler, Louis-Paul Henry, and Andreas M. Läuchli, "Observing the space- and time-dependent growth of correlations in dynamically tuned synthetic ising models with antiferromagnetic interactions," Phys. Rev. X **8**, 021070 (2018).

[52] Elmer Guardado-Sanchez, Peter T. Brown, Debayan Mitra, Trithep Devakul, David A. Huse, Peter Schauß, and Waseem S. Bakr, "Probing the quench dynamics of antiferromagnetic correlations in a 2d quantum ising spin system," Phys. Rev. X **8**, 021069 (2018).

[53] Sylvain de Léséleuc, Sebastian Weber, Vincent Lienhard, Daniel Barredo, Hans Peter Büchler, Thierry Lahaye, and Antoine Browaeys, "Accurate mapping of multilevel rydberg atoms on interacting spin-1/2 particles for the quantum simulation of ising models," Phys. Rev. Lett. **120**, 113602 (2018).

[54] R Coldea, D A Tennant, E M Wheeler, E Wawrzynska, D Prabhakaran, M Telling, K Habicht, P Smeibidl, and K Kiefer, "Quantum criticality in an ising chain: experimental evidence for emergent E8 symmetry," Science **327**, 177–180 (2010).

[55] Hyungwon Kim and David A. Huse, "Ballistic spreading of entanglement in a diffusive nonintegrable system," Phys. Rev. Lett. **111**, 127205 (2013).

[56] The said resonances for commensurable (J, h_z) are determined, strictly speaking, at vanishing transverse field. For finite $h_x \ll J$, the resonance points will be slightly shifted. This is illustrated, to some extent, in Fig. 1(c).

[57] Stefan Kühn, Erez Zohar, J. Ignacio Cirac, and Mari Carmen Bañuls, "Non-abelian string breaking phenomena with matrix product states," Journal of High Energy Physics **2015**, 130 (2015).

[58] T. Pichler, M. Dalmonte, E. Rico, P. Zoller, and S. Montangero, "Real-time dynamics in u(1) lattice gauge theories with tensor networks," Phys. Rev. X **6**, 011023 (2016).

[59] P. Sala, T. Shi, S. Kühn, M. C. Bañuls, E. Demler, and J. I. Cirac, "Variational study of u(1) and su(2) lattice gauge theories with gaussian states in $1+1$ dimensions," Phys. Rev. D **98**, 034505 (2018).

[60] Daniel Spitz and Jürgen Berges, "Schwinger pair production and string breaking in non-abelian gauge theory from real-time lattice improved hamiltonians," Phys. Rev. D **99**, 036020 (2019).

[61] Giuseppe Magnifico, Marcello Dalmonte, Paolo Facchi, Saverio Pascazio, Francesco V. Pepe, and Elisa Ercolessi, "Real Time Dynamics and Confinement in the $\mathbb{Z}_n$ Schwinger-Weyl lattice model for 1+1 QED," Quantum **4**, 281 (2020).

[62] Titas Chanda, Jakub Zakrzewski, Maciej Lewenstein, and Luca Tagliacozzo, "Confinement and lack of thermalization after quenches in the bosonic schwinger model," Phys. Rev. Lett. **124**, 180602 (2020).

[63] A. H. MacDonald, S. M. Girvin, and D. Yoshioka, "$\frac{t}{U}$ expansion for the hubbard model," Phys. Rev. B **37**, 9753–9756 (1988).

[64] Cheng-Ju Lin and Olexei I. Motrunich, "Quasiparticle explanation of the weak-thermalization regime under quench in a nonintegrable quantum spin chain," Phys. Rev. A **95**, 023621 (2017).

[65] Supplemental material for details on the perturbative derivation of the effective graph model and the solution of the quantum impurity model in the single-meson sector.

[66] Grégoire Misguich, Vincent Pasquier, and Jean-Marc Luck, "Inverse participation ratios in the xxz spin chain," Phys. Rev. B **94**, 155110 (2016).

[67] Alexander Cyril Hewson, *The Kondo Problem to Heavy Fermions*, Cambridge Studies in Magnetism (Cambridge University Press, 1993).

[68] A. J. Leggett, S. Chakravarty, A. T. Dorsey, Matthew P. A. Fisher, Anupam Garg, and W. Zwerger, "Dynamics of the dissipative two-state system," Rev. Mod. Phys. **59**, 1–85 (1987).

[69] Matthias Vojta, "Impurity quantum phase transitions," Philosophical Magazine **86**, 1807–1846 (2006), https://doi.org/10.1080/14786430500070396.

[70] Without loss of generality, we take the strength of the coupling between the impurity and the meson bath of the same order as the typical energy scale in the system, i.e. $O(T)$. See detailed discussion in Supp. Mat. [65].

[71] Andreas Sorge, "pyfssa 0.7.6." https://doi.org/10.5281/zenodo.35293.

[72] M.E.J. Newman and G.T. Barkema, *Monte Carlo Methods in Statistical Physics*, 1st ed. (Oxford University Press, New York, 1999).

[73] Roberto Verdel, Guo-Yi Zhu, and Markus Heyl, "Dynamical localization transition of string breaking in quantum spin chains: data," https://doi.org/10.5281/zenodo.7861807.

Supplemental Material

PERTURBATION THEORY FOR THE EFFECTIVE MODEL IN THE FOCK-SPACE GRAPH

In this section, we give a detailed derivation of the effective model in Eq. (4). We restrict ourselves to the limit of weak transverse fields, $h_x \ll J$. In this limit, it is convenient to write the Hamiltonian (1) as

$$\hat{H} = \hat{H}_0 + \hat{H}_1, \tag{S1}$$

where

$$\hat{H}_0 = -\sum_{i=1}^{L} \left(J\hat{\sigma}_i^z \hat{\sigma}_{i+1}^z + h_z \hat{\sigma}_i^z \right), \quad \hat{H}_1 = -h_x \sum_{i=1}^{L} \hat{\sigma}_i^x, \tag{S2}$$

and regard $\hat{H}_1$ as a small perturbation. Within this setting, we can perform a Schrieffer-Wolff (SW) transformation [63], i.e., a unitary transformation $e^{\hat{S}}$ to eliminate off-diagonal terms that do not preserve $\hat{H}_0$, order by order in the strength of the perturbation.

By choosing the generator of the transformation $\hat{S} = \hat{S}_1 + \hat{S}_2 + \cdots$, such that $[\hat{S}_1, \hat{H}_0] = -\hat{H}_1$, we get the following second-order Hamiltonian [32, 64]:

$$\hat{H}_2 = -\sum_i \left\{ \Delta_+ \hat{P}_{i-1}^\uparrow \hat{\sigma}_i^z \hat{P}_{i+1}^\uparrow + \Delta_- \hat{P}_{i-1}^\downarrow \hat{\sigma}_i^z \hat{P}_{i+1}^\downarrow + \Delta_0 \left(\hat{P}_{i-1}^\uparrow \hat{\sigma}_i^z \hat{P}_{i+1}^\downarrow + \hat{P}_{i-1}^\downarrow \hat{\sigma}_i^z \hat{P}_{i+1}^\uparrow \right) \right.$$
$$- (\Delta_+ - \Delta_0)\, \hat{P}_{i-1}^\uparrow (\hat{\sigma}_i^+ \hat{\sigma}_{i+1}^- + \text{h.c.}) \hat{P}_{i+2}^\uparrow - (\Delta_0 - \Delta_-)\, \hat{P}_{i-1}^\downarrow (\hat{\sigma}_i^+ \hat{\sigma}_{i+1}^- + \text{h.c.}) \hat{P}_{i+2}^\downarrow$$
$$\left. - (\Delta_- - \Delta_0)\, \hat{P}_{i-1}^\downarrow (\hat{\sigma}_i^+ \hat{\sigma}_{i+1}^+ + \text{h.c.}) \hat{P}_{i+2}^\downarrow \right\}, \tag{S3}$$

where $\hat{P}_i^{\uparrow(\downarrow)} = (\hat{1} \pm \hat{\sigma}_i^z)/2$ is the projector onto $\uparrow$ ($\downarrow$) at site i, and $\hat{\sigma}_i^\pm = (\hat{\sigma}_i^x \pm i\hat{\sigma}_i^y)/2$, are spin-$\frac{1}{2}$ raising and lowering operators. We have also introduced a succinct notation for the relevant energy scales: $\Delta_0 \equiv h_x^2/(2h_z)$, $\Delta_\pm \equiv h_x^2/(2h_z \pm 4J)$.

The ℓ-meson energies (with respect to the Ising vacuum energy), are obtained, to leading order, from the unperturbed Hamiltonian $\hat{H}_0$ and the diagonal terms on the r.h.s. of Eq. (S3). We get

$$m_1 = 4J + 2h_z + 2(2\Delta_+ - \Delta_0) + \mathcal{O}(h_x^4/J^3), \tag{S4}$$

$$m_{\ell \geq 2} = 4J + 2\ell h_z + (\ell + 2)\Delta_+ + (\ell - 2)\Delta_- + \mathcal{O}(h_x^4/J^3). \tag{S5}$$

We now focus on the situation of interest considered in the main text. Namely, $h_x \ll h_z = J$ and an initial string of size $\ell = 4$. The breaking of the string will necessarily yield the formation of two lighter mesons. Within the description above, the resonant decay channel (neglecting for a moment perturbative $(h_x/J)^2$ corrections) is into states with exactly two 1-meson particles, as it can be easily verified from Eqs. (S4) and (S5), for the relevant parameters. Hence, to the leading order, we can project the parent Hamiltonian onto the subsector of states with a single 4-meson particle ("string") and the subsector of two 1-meson states. By doing this, we get the effective model illustrated in Fig. 2 of the main text. Let us now explicitly write down the different terms of the this effective model. In the first place, we have the string and the 1-meson energies, which are given by

$$m_1 \approx 4J + 2h_z - \frac{h_x^2}{3J} = 6J - \frac{h_x^2}{3J}, \quad \mathcal{E}_s \equiv m_{\ell=4} \approx 4J + 8h_z = 12J. \tag{S6}$$

The latter term gives the first contribution in Eq. (4). Namely,

$$\hat{H}_{\text{string}}|S_j\rangle = \mathcal{E}_s|S_j\rangle, \tag{S7}$$

with the same notation for the ket $|S_j\rangle$ as in the main text. On the other hand, the 1-meson energy gives the diagonal part of $\hat{H}_{\text{mesons}}$ in Eq. (4), namely, $\hat{H}_{\text{mesons}}^{\text{diag}}|j,d\rangle = 2m_1|j,d\rangle$. We note however that this term has to be modified so as
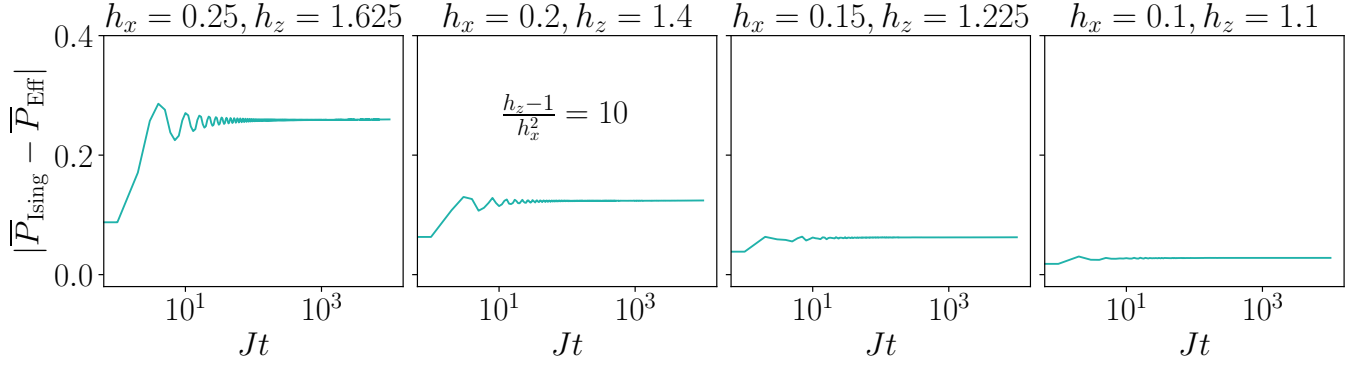
FIG. S1. Convergence of the effective model in the localized regime. Absolute error of the time-integrated string survival probability. The effective model becomes more accurate as h_x/J is reduced and h_z/J approaches 1, with $\frac{h_z-1}{h_x^2} = 10$ kept fixed. The values of the confining field h_z/J are such that they lead to localized string dynamics. Both h_x and h_z are in units of J. In all plots, we use $L = 14$ and $\ell = 4$.

to include a hardcore repulsive interaction between 1-meson particles, which arises from the second and third terms on the r.h.s. of Eq. (S3), namely, $U \equiv (2\Delta_0 - \Delta_-) = \frac{3h_x^2}{2J}$.

Next, we have to consider the off-diagonal terms on the r.h.s. of Eq. (S3). The first one of them, proportional to $\Delta_+ - \Delta_0$, acts as a hopping term for the 1-meson particles. This energy scale, therefore, defines the kinetic energy of such particles, $v \equiv -(\Delta_+ - \Delta_0) = \frac{h_x^2}{3J}$. Hence, $\hat{H}_{\mathrm{mesons}}$ in Eq. (4), acts on a 1-meson pair ket $|j, d\rangle$, as follows:

$$\hat{H}_{\mathrm{mesons}}|j,d\rangle = (2m_1 + \delta_{d,2}U)|j,d\rangle - v\Big[|j,d+1\rangle + |j+1,d-1\rangle + |j,d-1\rangle + |j-1,d+1\rangle\Big]. \tag{S8}$$

The last term on the r.h.s. of Eq. (S3), plays a crucial role in our description, for it describes the decay of a string of length $\ell = 4$ into a 1-meson pair, with a relative distance $d = 3$ and the position of the first $\downarrow$-spin in the latter configuration coinciding with that of the first $\downarrow$-spin in the former string configuration. This term also describes the reverse process of particle recombination into a single 4-meson particle. These two process are schematically illustrated by the green bond in Fig. 2(a). The numerical coefficient in front of this term thus sets the energy scale for the coupling $\hat{H}_\lambda$, namely, $\lambda \equiv (\Delta_- - \Delta_0) = -\frac{h_x^2}{J} = -3v$.

We note that the fifth term on the r.h.s. of Eq. (S3), yields no contribution when projecting onto the physically relevant subsectors for the case at hand. Furthermore, even though the derivation above holds strictly for $h_z = J$, it is possible to readily adjust the expressions above for $h_z \sim J$, by adding a straightforward h_z-dependent correction.

Since the system is translationally invariant, it is convenient to work in Fourier space. Using $|k,d\rangle = \frac{1}{\sqrt{L}} \sum_{j=1}^{L} e^{-ik(j+\frac{d}{2})}|j,d\rangle$, our effective model in momentum representation reads

$$\hat{\mathcal{H}} = \mathcal{E}_s \hat{I} + \sum_{k,d}(-2v + \delta_{d,2}U)|k,d\rangle\langle k,d| - 2v\sum_{k,d}\cos\left(\frac{k}{2}\right)\left(|k,d\rangle\langle k,d+1| + |k,d\rangle\langle k,d-1|\right)$$
$$- 3v\sum_{k,d}\delta_{d,3}\left(|S_k\rangle\langle k,d| + |k,d\rangle\langle S_k|\right), \tag{S9}$$

where k can take L possible values in the Brillouin zone $-\pi < k \leq \pi$, and the Kronecker delta in the last term is needed to appropriately couple a string configuration with the relevant state with two 1-mesons, as pointed out above.

While the effective model derived in this section is asymptotically exact as we let $h_x/J \to 0$ for the point $h_z = J$, it also yields accurate results for $h_z \neq J$. This is not only illustrated in Fig. 2(e) in the main text, but also in Fig. S1, which displays the absolute error (w.r.t. the full Ising model) of the time-integrated string survival probability for values of h_z/J that lead to localized string dynamics. We can see that our reduced model shows systematic convergence towards the exact dynamics in the Ising model, as we decrease h_x/J and let $h_z/J \to 1$ (while keeping the ratio $\frac{h_z-1}{h_x^2}$ fixed).

Let us also note that when we apply the SW transformation to rotate the Hamiltonian in order to eliminate off-diagonal terms, we should also rotate the initial state:

$$|\psi_0^{\mathrm{eff}}\rangle = e^{\hat{S}}|\psi_0\rangle = (1 - h_x\sum_i \hat{\sigma}_i^x + \cdots)|\cdots \uparrow\downarrow\downarrow\downarrow\downarrow\uparrow \cdots\rangle. \tag{S10}$$

Using $|\psi_0\rangle \equiv |\psi_{\text{string}}\rangle = |\cdots \uparrow\downarrow\downarrow\downarrow\uparrow \cdots\rangle$ as initial state for simulating the dynamics in the effective model will, instead, give us a $O(h_x/J)$-error. This error however is negligible when the survival probability is $P \sim 1$, but becomes more important when P is small. Nonetheless, for the considered timescales, we still obtain a very good agreement with the exact dynamics in the full Ising model.

EXACT SOLUTION OF THE QUANTUM IMPURITY MODEL IN THE DILUTE MESON LIMIT

Here we show how to solve the quantum impurity model in Eq. (6), in the single-meson limit. The single-meson sector is given by $\left\{ |S^z = 0\rangle \otimes |b_j^\dagger b_j = \delta_{j,j_0}\rangle, |S^z = \pm 1\rangle \otimes |b_j^\dagger b_j = 0\rangle \right\}$, for all j and for some $1 \leq j_0 \leq N$. The projected Hamiltonian is thus $\mathcal{P}\hat{H}_{\text{QIM}}\mathcal{P} \equiv \hat{\mathcal{H}}_{\text{QIM}}$. One can easily see that under this projection, the spin-1 degree of freedom representing the impurity can be replaced by two hard-core bosons with creation operators $\hat{a}_{\text{I}}^\dagger$, $\hat{a}_{\text{II}}^\dagger$, with the identification $n_{\text{I}} = 1 \leftrightarrow S^z = +1$ and $n_{\text{II}} = 1 \leftrightarrow S^z = -1$ (n_s being the eigenvalue of the occupation number $\hat{n}_s = \hat{a}_s^\dagger \hat{a}_s$; $s = \text{I, II}$). Therefore, we can consider a chain of $N + 2$ sites, with the extra two sites having labels I, II. This yields,

$$\hat{\mathcal{H}}_{\text{QIM}} = (M - \mu)(\hat{a}_{\text{I}}^\dagger \hat{a}_{\text{I}} + \hat{a}_{\text{II}}^\dagger \hat{a}_{\text{II}}) + \Lambda(\hat{a}_{\text{I}}^\dagger \hat{a}_{\text{I}} - \hat{a}_{\text{II}}^\dagger \hat{a}_{\text{II}}) + \sum_{j=1}^{N} \left[-T(\hat{b}_j^\dagger \hat{b}_{j+1} + \text{h.c.}) + (M - 2T)\hat{b}_j^\dagger \hat{b}_j \right]$$

$$- \frac{T}{\sqrt{2}} \left[(\hat{a}_{\text{I}}^\dagger + \hat{a}_{\text{II}}^\dagger)\hat{b}_1 + \text{h.c.} \right]. \tag{S11}$$

Furthermore, due to particle number conservation, the bilinear form above can exactly diagonalized for very large system sizes, and we can explicitly derive analytical expression for observables of interest. To show this, let us write this Hamiltonian in a compact way:

$$\hat{\mathcal{H}}_{\text{QIM}} = \sum_{i,j} \hat{c}_i^\dagger H_{i,j} \hat{c}_j, \tag{S12}$$

with $\hat{c}_i = \hat{a}_i, \hat{b}_i$, and where H is a Hermitian matrix (of dimension $N+2$), and hence, can be diagonalized by a unitary transformation $\mathcal{U}$:

$$\hat{c}_i^\dagger = \sum_{l=1}^{N+2} \hat{\alpha}_l^\dagger (\mathcal{U}^\dagger)_{li}, \quad \hat{c}_j = \sum_{l=1}^{N+2} \mathcal{U}_{jl} \hat{\alpha}_l. \tag{S13}$$

Thus, $\hat{H}_0$ simply reads

$$\hat{\mathcal{H}}_{\text{QIM}} = \sum_{l=1}^{N+2} \epsilon_l \hat{\alpha}_l^\dagger \hat{\alpha}_l. \tag{S14}$$

One can readily find that the creation/annihilation operators $\hat{\alpha}_l^\dagger, \hat{\alpha}_l$ evolve according to the following equations:

$$\hat{\alpha}_l^\dagger(t) = e^{i\epsilon_l t} \hat{\alpha}_l^\dagger, \quad \hat{\alpha}_l(t) = e^{-i\epsilon_l t} \hat{\alpha}_l. \tag{S15}$$

The initial string state in the quantum impurity model is given by $|\psi_0\rangle \equiv \frac{1}{\sqrt{2}}[|S^z = +1\rangle + |S^z = -1\rangle] \otimes |0\rangle_{\text{bath}}$, where $|0\rangle_{\text{bath}}$ is the vacuum state for the meson bath subsystem. In the language of the hard-core boson operators, this string state becomes:

$$|\psi_0\rangle = \frac{1}{\sqrt{2}} \left[\hat{a}_1^\dagger |0\rangle_{\text{imp}} + \hat{a}_2^\dagger |0\rangle_{\text{imp}} \right] \otimes |0\rangle_{\text{bath}}, \tag{S16}$$

where $|0\rangle_{\text{imp}}$ is the vacuum state of the impurity.

Thus, using the transformation in Eq. (S13) and the fact that $\hat{S}^z = \hat{a}_1^\dagger \hat{a}_1 - \hat{a}_2^\dagger \hat{a}_2$, we arrive at the following expression for the spin-spin autocorrelation function:

$$\langle \psi_0 | \hat{S}^z(t) \hat{S}^z(0) | \psi_0 \rangle = \frac{1}{2} \Bigg[u^+(1,1)u^-(1,1) - u^+(1,1)u^-(1,2) + u^+(2,1)u^-(1,1) - u^+(2,1)u^-(1,2)$$

$$- u^+(1,2)u^-(2,1) + u^+(1,2)u^-(2,2) - u^+(2,2)u^-(2,1) + u^+(2,2)u^-(2,2) \Bigg], \tag{S17}$$

Localization transition in the quantum impurity model
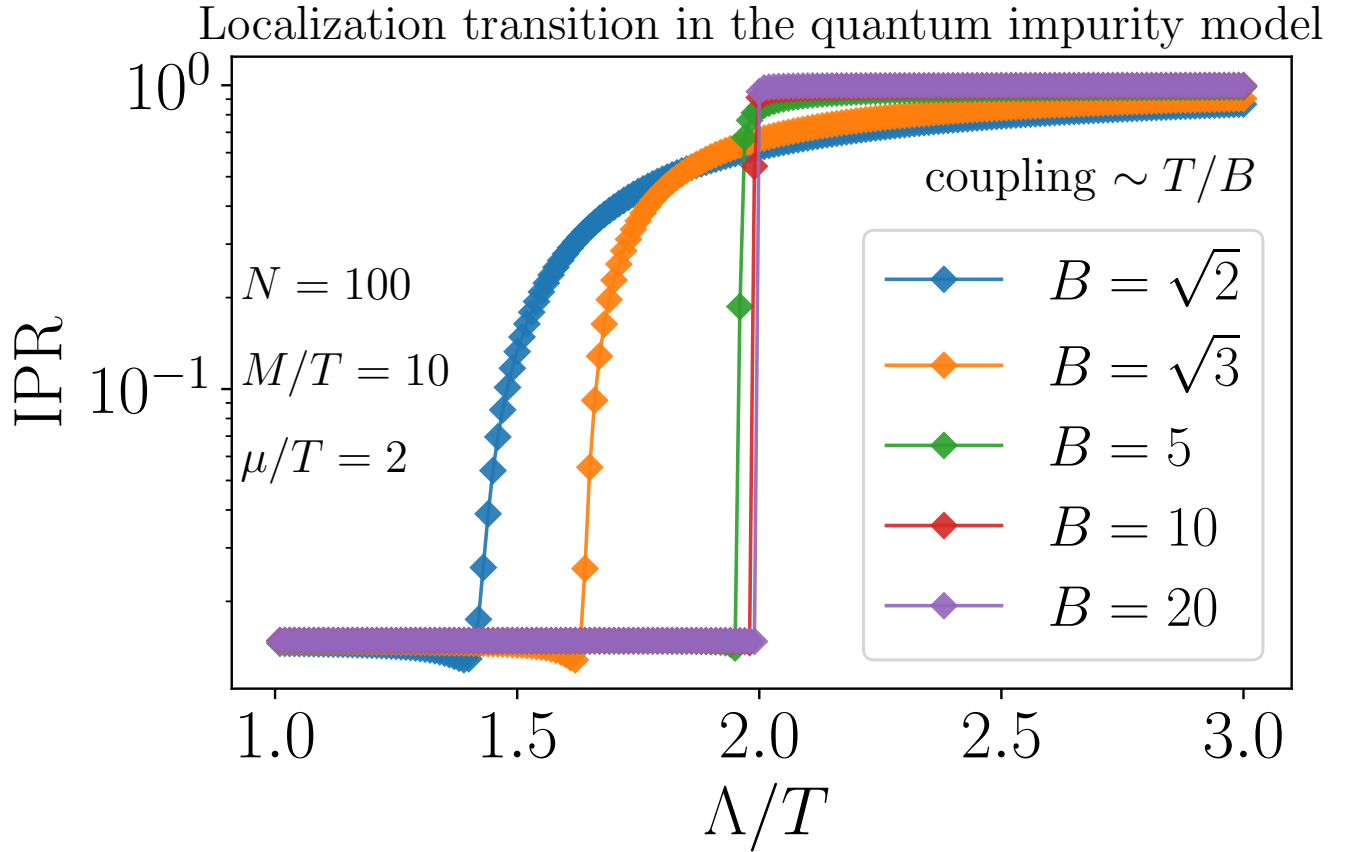
FIG. S2. Localization-delocalization transition in the generalized quantum impurity model for varying strength of the coupling. IPR of the lowest-lying eigenstate of the model in Eq. (S11) as a function of Λ/T. Here we explore the effect of adding a further free parameter B modulating the strength of the coupling term in our phenomenological description [last term in Eq. (S11)]. As the T/B is reduced the critical value of Λ/T converges to 2, as it can be readily understood from the cartoon picture in Fig. 3(a).

where $u^+(a,b) := \sum_l \mathcal{U}_{a,l} \mathrm{e}^{i\epsilon_l t}(\mathcal{U}^\dagger)_{l,b}$ and $u^-(a,b) := \sum_m \mathcal{U}_{a,m} \mathrm{e}^{-i\epsilon_m t}(\mathcal{U}^\dagger)_{m,b}$. This expression is used in the computation of the long-time average $\mathcal{M}(\Lambda)$.

As a final remark, we comment on how the localization-delocalization transition depends on the value of the coupling term in Eq. (S11). This is illustrated in Fig. S2, where we introduce a new parameter B modulating the strength of the said term. As the coupling between the impurity and the bath is decreased, we observe that the critical value of Λ/T approaches 2 (for the specific parameters used here, in particular, $\mu/T = 2$). Further, the transition becomes sharper and sharper. This can be easily understood from the cartoon picture drawn in Fig. 3(a), which precisely illustrates the limiting case of $B/T \to \infty$. At any rate, the overall qualitative result remains unaltered.